J. Fluid Mech. (2007), *vol.* 587, *pp.* 255–270. © 2007 Cambridge University Press
doi:10.1017/S0022112007007550 Printed in the United Kingdom

Turbulent flow on a planar moving belt and a rotating disk: modelling and comparisons

JOHN M. McDARBY AND FRANK T. SMITH

Dept. of Mathematics, University College London, Gower Street, London, WC1E 6BT, UK

(Received 8 September 2006 and in revised form 11 May 2007)

Modelling of the fully turbulent flow produced on a moving belt and of that induced on a rotating disk is described, for each of which a more analytical approach is adopted than previously seen. The analysis for the two-dimensional moving belt indicates novel structures and these are found to carry over directly to the rotating disk flow which, ignoring the transitional regime, is three-componential but two-dimensional due to axisymmetry. This is based on addressing the Reynolds-averaged Navier–Stokes equations together with an eddy viscosity model, with the flow structure being analysed for high Reynolds numbers. A classical (von Kármán) constant within the model plays an important and surprising role, indicating that each of the belt and the disk flows has quite a massive thickness. Comparisons made with previous work show varying degrees of agreement. The approach, including the new prediction of *massive thicknesses* independent of the Reynolds number, is expected to extend to flows induced by rotary blades, by related rotary devices and by other configurations of industrial interest.

1. Introduction

Rotating disk flow is our main concern here. The flow induced by a rotating disk is fundamental in theoretical terms for the laminar, transitional and turbulent regimes. The laminar state with its predicted axisymmetric flow pattern has been studied by von Karman (1921) and subsequently by many other authors: a clear overview is given by Zandbergen & Dijkstra (1987). It yields an exact solution of the Navier–Stokes equations and yet has some features which are quite representative of a full three-dimensional boundary layer, including crossflow effects in particular. Instability and transition from the laminar state are addressed by Gregory, Stuart & Walker (1955) and more recently Lingwood (1995, 1996), Davies & Carpenter (2003) and Davies, Thomas & Carpenter (2007) from various different and interesting perspectives. The fully turbulent state which is our central concern has been the subject of a significant range and variety of investigations, including Cooper (1971), Erian & Tong (1971), Launder & Sharma (1974), Cebeci & Abbott (1975), Littell & Eaton (1994) and Wu & Squires (2000). Further background references of note here include Prandtl (1952), Clauser (1956), and Schlichting (1960).

The theoretical rotating disk flow is also an attractive one concerning practical applications because it forms a convenient starting point for the context of complete rotor blade flow prediction by means of the cut-disk model. The completeness here refers to the capability of accommodating the entire spatially periodic motion produced by a rotary blade system rather than just the motion past an isolated blade. This aspect has enhanced interest in the area. The laminar regime for the cut disk is examined analytically and numerically in Smith & Timoshin (1996*a*), which shows

https://doi.org/10.1017/S0022112007007550 Published online by Cambridge University Press

the presence of a wide range of three-dimensional boundary layers with complicated crossflows and then leads on to the works of Smith & Timoshin (1996*b*), Bowles & Smith (2000*a*, *b*) and more recently Jones & Smith (2003) and Purvis & Smith (2004) including effects due to the proximity of the ground. Direct numerical solutions as described in Bhattacharrya & Smith (1996) tend to support the theoretical predictions. The turbulent flow regime in this context has attracted little if any attention however.

An approach similar to that used by Neish & Smith (1988) for the flow past a flat plate is found to be inappropriate for the flow past a rotating disk. In consequence, the turbulent flow past a flat plate with a moving surface is considered first. This is a simpler problem yet shares many of the key characteristics of the rotating disk flow and is therefore a useful starting point. As with the rotating disk, the flow over a planar moving surface has been the subject of a significant amount of research. Of this existing work, several studies warrant particular mention, most notably Sakiadis (1961*a*, *b*), Afzal (1996) and Tsou, Sparrow & Goldstein (1967). In particular the approach adopted by Afzal, specifically the use of an eddy viscosity model to analyse the turbulent boundary layer, is similar to the strategy used here although it should be noted that key differences emerge between our work and that of Afzal.

In this paper we present a novel structure for, along with analytical and numerical solutions to, the fully turbulent flows on a planar moving belt and a rotating disk, with results given for the components of the induced velocity, the displacement thickness and the skin friction. In § 2 the precise analysis used is discussed for the case of the planar moving belt (the analysis applies with minor modifications to a belt of finite or infinite length). In § 3 the natural extension of this method to the more complicated problem of a rotating disk is covered. For both the moving belt and rotating disk problems we begin with the Reynolds-averaged Navier–Stokes (RANS) equations taken with the Cebeci–Smith eddy viscosity model. Next a structure for the turbulent boundary layer is proposed which leads to the boundary layer being split into two coupled regions. A structure similar to that used by Mellor (1972), Bush & Fendell (1972) and Neish & Smith (1988) for the flow past a fixed flat plate in an outer stream is found to lead to a contradiction. The resolution of this problem requires an enhanced boundary layer where the thickness must be taken to be significantly larger than for flows driven by an outer stream. This phenomenon has been noted independently in a different context by Scheichl (2001) (see also Scheichl & Kluwick 2007*a*, *b*). Analytical and numerical solutions are then found for the velocity components in both layers, and these results are used to determine the displacement thickness. Lastly an analytical description of the skin friction is derived.

Finally, note that beyond the necessity of an increased boundary layer thickness, the model used here may seem essentially the same as that used previously, consisting of two coupled layers, an outer defect layer and a thinner wall layer (herein called the inertial-turbulent layer and the laminar sublayer respectively). Crucially though, the present increased thickness leads to a further difference between the turbulent boundary layers considered here and those examined previously, specifically that the outer, inertial-turbulent layer is found to be nonlinear, rendering an analytical solution in this region impossible in general.

2. A planar moving belt

To begin we consider a flat plate of length l, the surface of which moves with constant velocity U through a fluid which is otherwise at rest. Such a system can be pictured as similar to a moving conveyor belt although it is interesting to note

https://doi.org/10.1017/S0022112007007550 Published online by Cambridge University Press

that the experimental work of Tsou, Sparrow & Goldstein (1967) used a rotating cylindrical drum (which was sufficiently large for the effects of curvature to be negligible) to create a planar moving surface. Here the flow is taken to be two-dimensional and Cartesian coordinates x_D and y_D are used, where x_D measures distance along the surface of the plate and y_D measures height above the plate. The corresponding velocity components are u_D and v_D respectively with boundary conditions $u_D(x_D, 0) = U$ and $u_D(x_D, y_D \to \infty) = 0$. The governing equations for this flow are the time-averaged Navier–Stokes equations. These can be simplified in the present flow configuration through the use of the boundary layer approximation, as described below, with the Reynolds stress modelled by a suitable eddy viscosity model. In particular an algebraic model has been chosen (rather than a one- or two-equation model) because of the relative simplicity and clarity of such an approach which, in view of the need for a numerical solution and analytical comparison, are considered important. Our particular choice of algebraic model – Cebeci–Smith (see Speziale & So 1998 and Wilcox 1998) – has been used successfully in a variety of related flows and so is selected as a suitable model for use here. Although the Cebeci–Smith eddy viscosity does have limitations, not least that it assumes isotropic turbulence, since the main focus of the present work is to develop an analytical approach to the planar moving belt flow such simplifications are considered acceptable. Hence we have

$$u_D \frac{\partial u_D}{\partial x_D} + v_D \frac{\partial u_D}{\partial y_D} = \nu \frac{\partial^2 u_D}{\partial y_D^2} + \frac{\partial}{\partial y_D} \begin{cases} k_2 U \delta_D^* \dfrac{\partial u_D}{\partial y_D} & \text{for } y_D \geqslant y_{Dk} \\ -k_1^2 {y_D}^2 \left[1 - \exp\left(-\dfrac{y_D u_{\tau D}}{26\nu}\right)\right]^2 \left(\dfrac{\partial u_D}{\partial y_D}\right)^2 & \text{for } y_D \leqslant y_{Dk}, \end{cases} \tag{2.1}$$

where $\delta_D^* = \int_0^\infty (u_D/U)\mathrm{d}y_D$ is the displacement thickness of the boundary layer, $u_{\tau D} = \sqrt{|(\tau_{WD}/\rho)|}$ is the friction velocity and $\tau_{WD} = \mu(\partial u_D/\partial y_D)_{y_D=0}$ is the shear stress on the belt. The constants k_1 and k_2 are 0.4 and 0.0168 respectively. The height of the boundary layer is taken to be $O(k_1^2)$ and hence we require $k_1^2 \ll 1$ in order to define the boundary layer itself, which is therefore of massive thickness. It is also assumed that $k_2 = O(k_1^2)$, which is a reasonable estimate.

Equation (2.1) is simplified through the use of the quasi-similarity solution $u_D = Uf'(z)$ where $z = y_D/(k_1^2 x_D)$ (in this context the term quasi-similarity solution is used because the variable z is still dependent on x_D). This leads to

$$-ff'' = \frac{1}{R} f''' + \frac{\mathrm{d}}{\mathrm{d}z} \begin{cases} k_3 f_\infty f'' & \text{for } z \geqslant z_k \\ -z^2 \left[1 - \exp\left(-\frac{1}{26} z u_\tau\right)\right]^2 f''^2 & \text{for } z \leqslant z_k \end{cases} \tag{2.2}$$

where $R = k_1^4 U x_D/\nu = k_1^4 Re$, $u_{\tau D} = k_1^2 U u_\tau$ and $k_3 = k_2/k_1^2 = 0.105$. The boundary conditions are now $f(0) = 0$, $f'(0) = 1$ and $f'(\infty) = 0$.

Flow structure

In the case of turbulent flow past a stationary flat plate the decreasing influence of viscosity as distance from the plate increases leads to the well-established (see Mellor 1972, Bush & Fendell 1972 and others) model which regards the boundary layer as being composed of two layers with distinct characteristics. Although this structure is typically applied to flows driven by a free stream rather than the surface-driven flows examined here, it is argued that the physics of both layers is essentially the same and hence the same model can be applied. Specifically, the argument applied

https://doi.org/10.1017/S0022112007007550 Published online by Cambridge University Press

in free-stream-driven flows that as distance from the surface decreases fluid velocities tend to zero and so viscous effects dominate over the inertial terms, can be replaced by the argument that as distance from the plate decreases the fluid flow becomes increasingly invariant to tangential position. This has the same effect as a decreasing velocity, namely that the inertial terms become small close to the surface allowing viscosity to dominate (although it should be noted that this argument does not apply fully to the rotating disk flow and hence the retention of an inertial effect in the laminar sublayer in that case). Moreover the belt effect is very similar to that of a stream acting at the lower edge of the outer layer rather than at its upper edge. Furthermore, whilst the two-layer structure is herein applied to the boundary layer equations this is simply a consequence of scaling and we are investigating the full RANS equations, for which this model was originally devised.

The two-layer approach has been used successfully in many problems (for instance Neish & Smith 1988 and Afzal 1996) yet when a classical formulation is applied to the present flow (and indeed to the rotating disk flow also) a contradiction arises. The resolution to this is to increase the size of the outer layer so that, relative to typical boundary layers, it is of *massive thickness*. A similar result was found independently by Scheichl (2001) concerning turbulent jets. Hence we view the boundary layer as being composed of one relatively thick outer region in which viscosity is negligible, known here as the inertial-turbulent layer, and a second thin layer attached to the plate, known as the laminar sublayer.

We begin by considering the inertial-turbulent layer where, noting the enhanced thickness of this outer layer, the following scalings apply; $f' = \epsilon f_1' + \cdots$ and $z = O(1)$, where $\epsilon = (\ln R)^{-1}$. Hence for the flow in the inertial-turbulent layer we arrive at the controlling equation

$$-f_1 f_1'' = \frac{\mathrm{d}}{\mathrm{d}z}\begin{cases} k_3 f_{1\infty} f_1'' & \text{for } z \geqslant z_k \\ -z^2 f_1''^2 & \text{for } z \leqslant z_k, \end{cases} \tag{2.3}$$

with $f_1(0) = 0$ and $f_1'(\infty) = 0$. It should be noted that the enhanced boundary layer thickness here leads to an $O(\epsilon)$ velocity in this outer layer, to leading order, rather than the $O(1)$ outer layer velocity seen in Afzal (it is also noted that we retain both forms of the eddy viscosity in our outer layer whereas Afzal only uses the upper form).

In the laminar sublayer we take $z = O(\epsilon^{-1}R^{-1})$ (see Neish & Smith 1988) and so $f' = 1 + \epsilon f_2' + \cdots$ and $z = \epsilon^{-1}R^{-1}z_2 + \cdots$ where f_2' and z_2 are $O(1)$. Hence to leading order (2.2) becomes

$$f_2''' - \frac{\mathrm{d}}{\mathrm{d}z_2}\left(z_2^2\left[1 - \exp\left(-\frac{z_2 u_\tau}{26\epsilon}\right)\right]^2 f_2''^2\right) = 0. \tag{2.4}$$

Integrating (2.4) then leads to the shear result

$$f_2'' - z_2^2\left[1 - \exp\left(-\frac{z_2 u_\tau}{26\epsilon}\right)\right]^2 f_2''^2 = -C_1^2, \tag{2.5}$$

where C_1 is a constant, suggesting that $f_2' \sim C_1 \ln z_2$ as $z_2 \to \infty$; in particular logarithmic matching of the solutions in each layer leads to $f' = 1 + \epsilon f_2' \sim 1 - \epsilon \ln z_2$ as $z_2 \to \infty$ (and thus $C_1 = -1$), and as $z \to 0$ $f' = \epsilon f_1'(z) \sim -\epsilon \ln z$. It is now possible to consider each region separately and so the solution is constructed in two parts: first a mainly analytical solution for the laminar sublayer and then a numerical solution for the inertial-turbulent layer.

https://doi.org/10.1017/S0022112007007550 Published online by Cambridge University Press

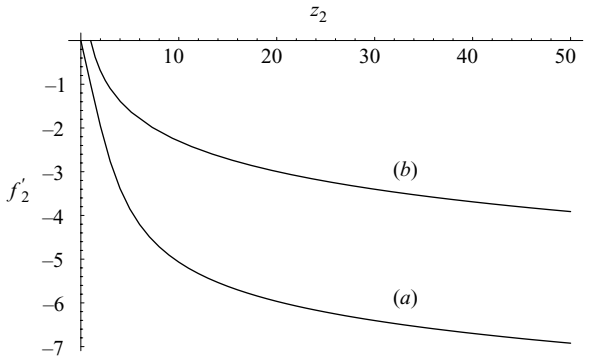


FIGURE 1. (*a*) Analytical solution for $f_2'(z_2)$ in the laminar sublayer. (*b*) Plot of $-\ln z_2$.

Flow solution in the laminar sublayer

Without loss of generality, (2.5) can be rearranged and solved in the form

$$\alpha_2^2(z_2) - F(z_2)\alpha_2(z_2) - F(z_2) = 0. \tag{2.6}$$

Here $\alpha_2(z_2) = f_2''(z_2)$, $F(z_2) = z_2^{-2}[1 - \exp(-z_2 u_\tau/(26\epsilon))]^{-2}$ and $u_\tau = \epsilon/k_1$, the verification of which follows later (we note that ϵ, and hence u_τ, decays with x_D as $R = k_1^4 U x_D/\nu$ and $\epsilon = (\ln R)^{-1}$). Hence $\alpha_2 = \frac{1}{2}(F - \sqrt{(F^2 + 4F)})$. Integrating $\alpha_2(z_2)$ numerically, with $f_2'(0) = 0$, leads to the solution illustrated in figure 1, along with a plot of $-\ln z_2$ for comparison. The solution suggests the asymptotic form

$$f_2' \sim -\ln z_2 - 3.0 \tag{2.7}$$

as $z_2 \to \infty$, where the constant term (3.0 to two significant figures) in the asymptote comes from examining the numerical solution for f_2' at large values of z_2. This compares well with the work of Afzal (1996) whose results can be rearranged (see McDarby 2004) to give the following asymptotic behaviour:

$$f_2' \sim -\ln z_2 - 2.9. \tag{2.8}$$

Flow solution in the inertial-turbulent layer

The nonlinear inertial-turbulent layer requires a numerical treatment of (2.3). A solution is obtained using a shooting method, based on a Runge–Kutta–Fehlberg algorithm. The substitutions $z = z_k t$, $f_1 = f_{1\infty} a(t)$, $f_1'(z) = f_{1\infty} b(t)$ and $f_1''(z) = f_{1\infty} c(t)$ are introduced into (2.3), which then becomes the following three first-order equations:

$$\frac{\mathrm{d}a}{\mathrm{d}t} = b, \tag{2.9}$$

$$\frac{\mathrm{d}b}{\mathrm{d}t} = c, \tag{2.10}$$

$$\frac{\mathrm{d}c}{\mathrm{d}t} = -Kac, \tag{2.11}$$

with the relevant boundary conditions $a(\infty) = 1$, $b(\infty) = 0$ and $c(\infty) = c_\infty$, for the range $t \geqslant 1$, with $K = z_k/k_3$ and c_∞ to be determined numerically. In practice the boundary conditions at infinity are replaced by the same boundary conditions at a finite height, denoted t_∞. Numerical results are then calculated at increasing values of t_∞ until further increases produce only a negligible change in the results obtained (the value $t_\infty = 30$ is used in all subsequent calculations).

https://doi.org/10.1017/S0022112007007550 Published online by Cambridge University Press

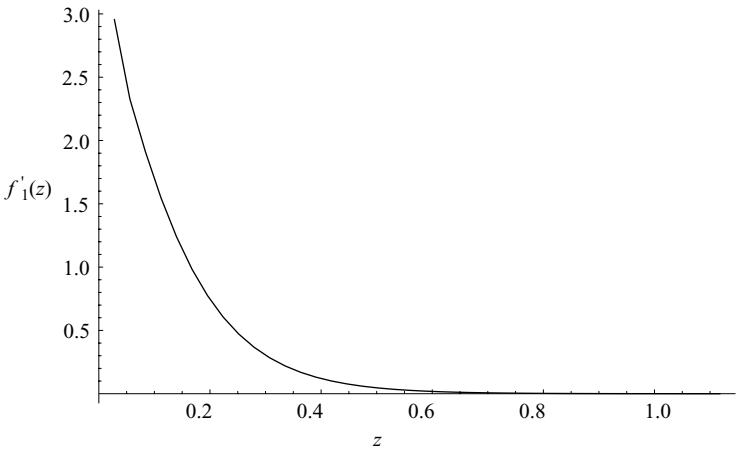


FIGURE 2. Velocity profile for the flow in the inertial-turbulent layer, $f_1'(z)$, where z is the quasi-similarity variable.

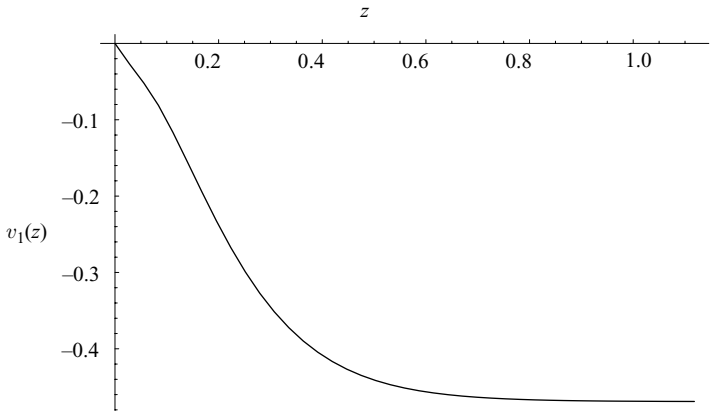


FIGURE 3. Normal velocity profile for the flow in the inertial-turbulent layer, $v_1 = zf_1' - f_1$, where z is the quasi-similarity variable.

We also have

$$\frac{\mathrm{d}a}{\mathrm{d}t} = b, \tag{2.12}$$

$$\frac{\mathrm{d}b}{\mathrm{d}t} = c, \tag{2.13}$$

$$\frac{\mathrm{d}c}{\mathrm{d}t} = \frac{(Ja - tc)}{t^2}, \tag{2.14}$$

with the boundary condition $a(0) = 0$, for the range $0 \leqslant t \leqslant 1$, with $J = \frac{1}{2}z_k$. We require continuity of a, b and c at $t = 1$, as well as $c(1) = -k_3$ which represents continuity of the eddy viscosity at $z = z_k$.

The subsequent solutions generated for $f_1'(z)$ and v_1, the non-dimensional normal velocity component, are shown in figures 2 and 3 and yield the values $f_{1\infty} = 0.469$ and $z_k = 0.056$. More importantly these results can now be used to determine velocity profiles and values for the displacement thickness and skin friction on the belt and these predictions will now be presented alongside existing experimental, analytical

https://doi.org/10.1017/S0022112007007550 Published online by Cambridge University Press

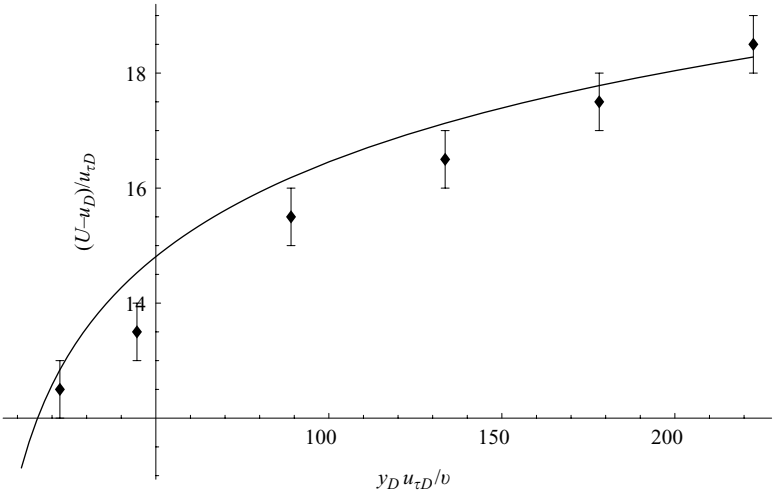


FIGURE 4. Predicted velocity profile for the law of the wall compared with the experimental results of Tsou, Sparrow & Goldstein (1967). The curve represents the present predictions whilst the error bars are an approximate representation of the results of Tsou, Sparrow & Goldstein (1967) at various points. The horizonal axis measures the scaled height $y_D u_{\tau D}/\nu$ and the vertical axis measures $(U - u_D)/u_{\tau D}$.

and numerical results. Before proceeding to illustrate and discuss the results of this paper it is worth calling attention to the comparisons drawn to earlier work. Where possible existing analytical results are shown alongside the present findings whilst in the case of experimental data, and in the absence of such original information, estimates of other authors' findings are included along with reference to the source text. In such cases these estimates are presented as a range rather than a precise value.

Velocity profile

Our results are now compared to those of Tsou, Sparrow & Goldstein (1967) concerning the law of the wall for the behaviour of the velocity near the moving belt, as shown in figure 4. Although some discrepancies are apparent, the present results are broadly in agreement with those of Tsou *et al.*

Displacement thickness

Next the displacement thickness δ_D^* can be determined from our numerical results:

$$\delta_D^* = \int_0^\infty \frac{u_D}{U}\,\mathrm{d}y_D = k_1^2 \epsilon\, f_{1\infty} x_D. \tag{2.15}$$

To leading order the values for displacement thickness are shown in figure 5 along with the results of Sakiadis. It is clear that whilst our predictions for the displacement thickness are of a similar magnitude, the present results suggest a different growth to that of Sakiadis. This may be a consequence of our use of a quasi-similarity solution and Sakiadis' assumption of a $\frac{1}{7}$-power velocity profile. Sakiadis' results for the displacement thickness on a flat plate in a moving stream are included as an illustration of the enhanced boundary layer thickness found on a planar moving belt.

https://doi.org/10.1017/S0022112007007550 Published online by Cambridge University Press

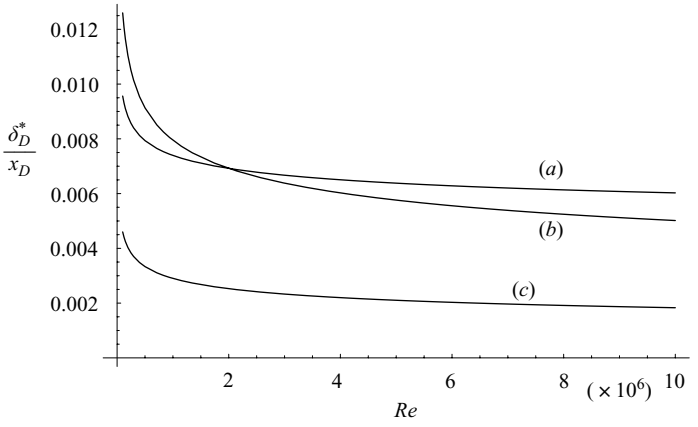


FIGURE 5. Comparison of our predictions (*a*) for the displacement thickness with those of Sakiadis (1961*b*) for a continuous flat plate with a moving surface (*b*) and a finite plate in a moving stream (*c*).

Skin friction

Finally we turn our attention to the skin friction on the belt. In particular, (2.5) permits an analytic solution. As $z_2 \to 0$, (2.5) yields

$$f_2'' \to -1. \tag{2.16}$$

Hence

$$\frac{\partial u_D}{\partial y_D} \to -\frac{U\epsilon^2 R}{k_1^2 x_D}. \tag{2.17}$$

The skin friction is defined as

$$c_f = \frac{2\tau_{WD}}{\rho U^2} = \frac{2\mu(|\partial u_D/\partial y_D|)_{y_D=0}}{\rho U^2}. \tag{2.18}$$

Hence the following form for the skin friction c_f is obtained:

$$c_f = 2k_1^2\epsilon^2, \tag{2.19}$$

as illustrated in figure 6. These results exhibit very close agreement with Afzal (1996) (we note that the skin friction decays with x_D as $R = k_1^4 U x_D/\nu$ and $\epsilon = (\ln R)^{-1}$). It also follows that since $u_\tau = u_{\tau D}/(k_1^2 U)$ and $\tau_{WD} = \rho u_{\tau D}^2$, then from (2.18) and (2.19) we have $u_\tau = \epsilon/k_1$ as stated previously.

Summary

The application of the relatively large outer layer matched with a conventional laminar sublayer has led to analytical and numerical results which display promising agreement with existing work. In particular, the simplification that this leads to in the laminar sublayer enables us to derive a (mostly) analytic solution for the platewise velocity and an analytic prediction for the skin friction, both of which closely match similar work by Afzal. The solution of the flow in the inertial-turbulent layer remains a more complicated nonlinear problem although our method has produced results which are satisfactory. Where disagreements arise, in particular with the mixed analytical/numerical approach taken by Sakiadis, these may be explained by the use of simplifying assumptions; in the case of the present work this is the use of a quasi-similarity solution; in the case of Sakiadis, a $\frac{1}{7}$-power law for the velocity profile.

https://doi.org/10.1017/S0022112007007550 Published online by Cambridge University Press

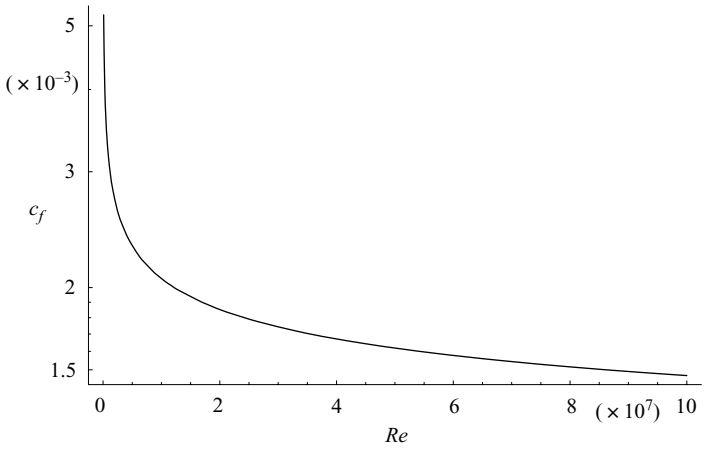


FIGURE 6. Current predictions for the skin friction on a moving belt.

The promising agreement between the present findings and those of other authors also serves as validation of the use of the Cebeci–Smith model for this flow. Note also that our predictions for the velocity in the laminar sublayer and for the skin friction on the plate depend on the asymptotic behaviour of the eddy viscosity rather than on its exact form and so these results, and the general analysis applied here, are expected to carry over to other models of the eddy viscosity.

3. Rotating disk

As stated earlier, the fully turbulent flow due to a rotating disk is the principle concern of the present work and so the approach used in § 2 is now extended to the flow over a disk rotating in an otherwise stationary and unbounded fluid. This problem has been the subject of a wide variety of previous investigations including experimental studies (Erian & Tong 1971 and Littell & Eaton 1994) and numerical solutions involving the use of an eddy viscosity model (Cooper 1971 and Cebeci & Abbott 1975), an energy-dissipation model (Launder & Sharma 1974) and large-eddy simulation (Wu & Squires 2000). The present investigation will adopt a similar starting point to that of Cooper in that we also use the RANS equations simplified by the boundary layer approximation and the Cebeci–Smith eddy viscosity model; however our approach will differ from that of Cooper as we seek a more analytical solution and unlike Cooper we will ignore intermittency. The findings of other authors are also important to our work and where appropriate will be compared with the current predictions.

For convenience cylindrical polar coordinates r_D, θ and z_D are used where u_D,v_D and w_D are the velocity components in the radial, azimuthal and normal directions respectively. Assuming that the flow is steady and axisymmetric we arrive at the following governing equations:

$$u_D\frac{\partial u_D}{\partial r_D}-\frac{v_D^2}{r_D}+w_D\frac{\partial u_D}{\partial z_D}=\nu\frac{\partial^2 u_D}{\partial {z_D}^2}+\frac{\partial}{\partial z_D}\left(\nu_{tD}\frac{\partial u_D}{\partial z_D}\right), \tag{3.1}$$

$$u_D\frac{\partial v_D}{\partial r_D}+\frac{u_D v_D}{r_D}+w_D\frac{\partial v_D}{\partial z_D}=\nu\frac{\partial^2 v_D}{\partial {z_D}^2}+\frac{\partial}{\partial z_D}\left(\nu_{tD}\frac{\partial v_D}{\partial z_D}\right), \tag{3.2}$$

https://doi.org/10.1017/S0022112007007550 Published online by Cambridge University Press

and continuity equation

$$\frac{1}{r_D}\frac{\partial(u_D r_D)}{\partial r_D} + \frac{\partial w_D}{\partial z_D} = 0. \tag{3.3}$$

Now the eddy viscosity is defined as

$$\nu_{tD} = \begin{cases} k_2 \omega r_D \delta_D^*, & z_D \geqslant z_{Dk} \\ k_1^2 z_D^2 \left[1 - \exp\left(- \frac{z_D}{26\nu}\left|\frac{\tau_{WD\theta}}{\rho}\right|^{1/2}\right)\right]^2 \left|\frac{\partial u_D}{\partial z_D} + \frac{\partial v_D}{\partial z_D}\right|, & z_D \leqslant z_{Dk}, \end{cases} \tag{3.4}$$

where ω is the angular velocity of the disk and the constants k_1 and k_2 are again 0.4 and 0.0168 respectively. The displacement thickness δ_D^* is

$$\delta_D^* = \int_0^\infty \frac{v_D}{\omega r_D} \mathrm{d}z_D, \tag{3.5}$$

and the shear stress on the disk, $\tau_{WD\theta}$, is given by

$$\tau_{WD\theta} = \mu \left(\frac{\partial v_D}{\partial z_D}\right)_{z_D=0}. \tag{3.6}$$

The boundary conditions are $u_D(r_D, \theta, 0) = 0$, $v_D(r_D, \theta, 0) = \omega r_D$ and $u_D(r_D, \theta, z_D \to \infty) = v_D(r_D, \theta, z_D \to \infty) = 0$. Like the flow past a moving belt, the height of the boundary layer is taken to be $O(k_1^2)$ where $k_1^2 \ll 1$ and a quasi-similarity solution for the whole of the turbulent boundary layer is sought by introducing the substitutions

$$u_D = \omega r_D f'\left(z_D/k_1^2 r_D\right), \tag{3.7}$$

$$v_D = \omega r_D g'\left(z_D/k_1^2 r_D\right), \tag{3.8}$$

with a prime denoting differentiation with respect to $\eta = z_D/k_1^2 r_D$. These lead to the following form for the normal velocity: $w_D = -\omega k_1^2 r_D (3f - \eta f')$. The conditions $f(0) = g(0) = 0$ can be set without loss of generality.

The system is therefore reduced to the following pair of coupled nonlinear ordinary differential equations,

$$f'^2 - 3ff'' - g'^2 = \frac{1}{R} f''' + \frac{\mathrm{d}}{\mathrm{d}\eta} \begin{cases} k_3 g_\infty f'', & \eta \geqslant \eta_k \\ \eta^2 \left[1 - \exp\left(-\frac{1}{26}\eta R u_\tau\right)\right]^2 (f''^2 + g''^2)^{1/2} f'', & \eta \leqslant \eta_k, \end{cases} \tag{3.9}$$

and

$$2f'g' - 3fg'' = \frac{1}{R} g''' + \frac{\mathrm{d}}{\mathrm{d}\eta} \begin{cases} k_3 g_\infty g'', & \eta \geqslant \eta_k \\ \eta^2 \left[1 - \exp\left(-\frac{1}{26}\eta R u_\tau\right)\right]^2 (f''^2 + g''^2)^{1/2} g'', & \eta \leqslant \eta_k. \end{cases} \tag{3.10}$$

Here $u_{\tau D} = k_1^2 \omega r_D u_\tau$ and $R = k_1^4 \omega r_D^2/\nu = k_1^4 R_r$, where R and R_r are the normalized rotational and the rotational Reynolds numbers respectively.

Flow structure

Again the turbulent boundary layer is regarded as being composed of two distinct layers with heights $O(1)$ and $O(\epsilon^{-1}R^{-1})$ respectively. In the inertial-turbulent layer $f' = \epsilon f_1' + \cdots$, $g' = \epsilon g_1' + \cdots$ and $\eta = O(1)$ with $\epsilon = (\ln R)^{-1}$. Hence (3.9) and (3.10)

https://doi.org/10.1017/S0022112007007550 Published online by Cambridge University Press

reduce to

$$f_1'^2 - 3f_1 f_1'' - g_1'^2 = \frac{\mathrm{d}}{\mathrm{d}\eta}\begin{cases} k_3 g_{1\infty} f_1'', & \eta \geqslant \eta_k \\ \eta^2\left(f_1''^2 + g_1''^2\right)^{1/2} f_1'', & \eta \leqslant \eta_k, \end{cases} \tag{3.11}$$

and

$$2f_1' g_1' - 3f_1 g_1'' = \frac{\mathrm{d}}{\mathrm{d}\eta}\begin{cases} k_3 g_{1\infty} g_1'', & \eta \geqslant \eta_k \\ \eta^2\left(f_1''^2 + g_1''^2\right)^{1/2} g_1'', & \eta \leqslant \eta_k. \end{cases} \tag{3.12}$$

The viscous term is neglected here and since $\eta = O(1)$ the exponential term in the lower form of the eddy viscosity is sufficiently small to be ignored.

In the laminar sublayer, $g' = 1 + \epsilon g_2' + \cdots$ to match with the inertial-turbulent layer and to satisfy the boundary condition on the surface, while the scaling $\eta = \epsilon^{-1} R^{-1} \eta_2$ is required to ensure a balance between the viscous and turbulent terms. Also we expect $f' = \epsilon^{-2} R^{-1} f_2' + \cdots$ in order to retain an inertial effect in the radial momentum balance. This is necessary to avoid a zero radial flow as $\eta_2 \to \infty$ which cannot match with the radial velocity in the inertial-turbulent layer. Since $|g''| \gg |f''|$, and assuming monotonic decay in the azimuthal velocity, so that $g'' < 0$, it follows that $\sqrt{(f''^2 + g''^2)} = -g''$ to leading order. Consequently the above substitutions lead to the governing system

$$-1 = f_2''' - \frac{\mathrm{d}}{\mathrm{d}\eta_2}\left(\eta_2^2\left[1 - \exp\left(-\frac{\eta_2}{26\epsilon} u_\tau\right)\right]^2 g_2'' f_2''\right), \tag{3.13}$$

$$0 = g_2''' - \frac{\mathrm{d}}{\mathrm{d}\eta_2}\left(\eta_2^2\left[1 - \exp\left(-\frac{\eta_2}{26\epsilon} u_\tau\right)\right]^2 g_2''^2\right). \tag{3.14}$$

The motion here is predominantly two-dimensional with an additional crossflow. Equation (3.14) implies logarithmic behaviour as $\eta_2 \to \infty$ and again it is necessary to match the solution for the inertial-turbulent layer with the asymptotic logarithmic behaviour in the laminar sublayer. Hence, as $\eta \to 0$, $f' = \epsilon f_1'(\eta) \sim -\epsilon\eta(\ln\eta)^2$ and $g' = \epsilon g_1'(\eta) \sim -\epsilon \ln\eta$ whilst as $\eta_2 \to \infty$, $f' = \epsilon^{-2} R^{-1} f_2'(\eta_2) \sim -\epsilon^{-2} R^{-1} \eta_2$ and $g' = 1 + \epsilon g_2'(\eta_2) \sim 1 - \epsilon \ln \eta_2$.

Flow solution in the laminar sublayer

The approach used to derive an analytical solution to the flow in the laminar sublayer on a moving belt is repeated here for the azimuthal velocity component and leads to

$$g_2' \sim -\ln \eta_2 - 3.0. \tag{3.15}$$

Flow solution in the inertial-turbulent layer

The substitutions $\eta = \eta_k t$, $f_1 = g_{1\infty} s_1$, $f_1' = g_{1\infty} s_2$, $f_1'' = g_{1\infty} s_3$, $g_1 = g_{1\infty} s_4$, $g_1' = g_{1\infty} s_5$ and $g_1'' = g_{1\infty} s_6$ are introduced into (3.11) and (3.12) leading to two sets of first-order equations. As with the flow on a flat plate the boundary conditions at infinity are replaced with the same conditions applied at a finite height, t_∞. The same iterative numerical approach that was used in the moving belt flow is extended to the current more complicated problem, generating the solutions illustrated in figures 7, 8 and 9. This approach leads to $g_{1\infty} = 0.217$ and $\eta_k = 0.027$.

It should be noted that for the calculations presented here $t_\infty = 20$. Increasing the value of t_∞ leads to only a negligible change in the numerical results obtained, except for a small but noticeable difference in the radial velocity component at large values of t. In particular the radial velocity component is seen to decay more slowly as t_∞ is increased. Results could be calculated at a much larger value of t_∞ to produce

https://doi.org/10.1017/S0022112007007550 Published online by Cambridge University Press

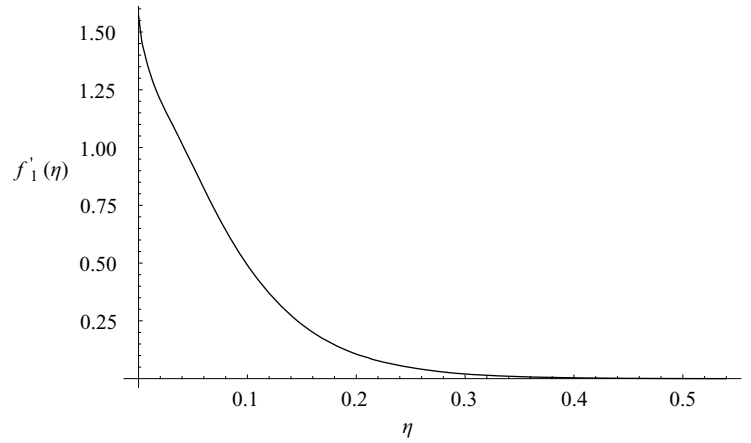


FIGURE 7. Radial velocity profile for $f_1'(\eta)$, where η is the quasi-similarity variable.

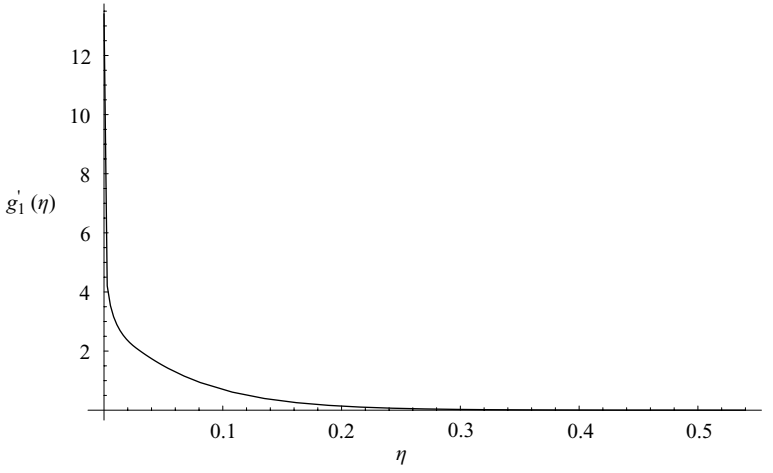


FIGURE 8. Azimuthal velocity profile for $g_1'(\eta)$, where η is the quasi-similarity variable.

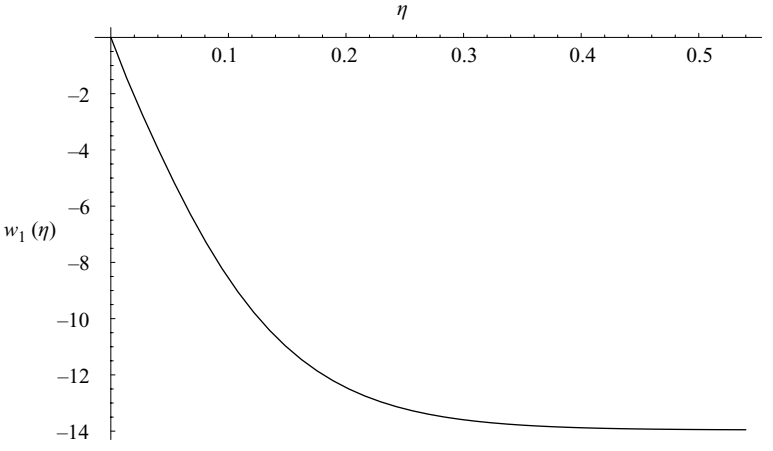


FIGURE 9. Non-dimensional normal velocity, $w_1 = -3f_1 + \eta f_1'$, on a rotating disk.

https://doi.org/10.1017/S0022112007007550 Published online by Cambridge University Press

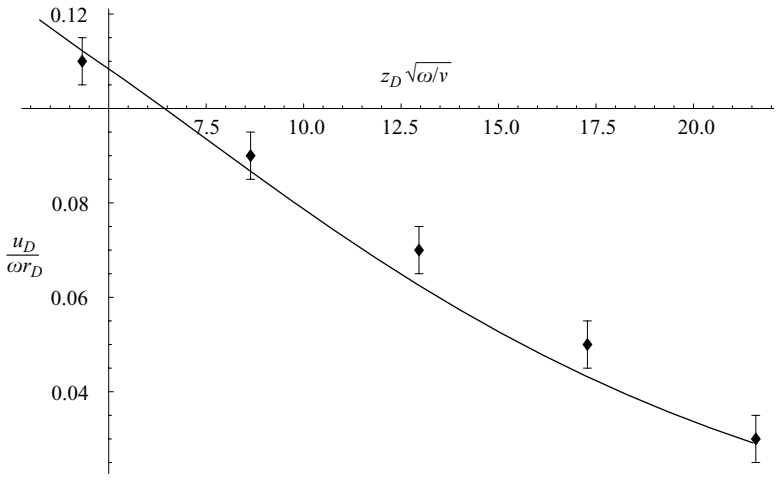


FIGURE 10. Radial velocity profile on a rotating disk compared with the work of Erian & Tong (1971). The current predictions are shown as a curve whilst the results of Erian & Tong at various points are included as error bars, indicating the range in which their results lie as accurately as is possible.

more accurate predictions for the radial velocity far from the disk; however, given the significant increase in computation that is then required to produce a relatively small improvement in the overall accuracy of the results, $t_\infty = 20$ is deemed to be the most appropriate value to use.

Velocity profiles

Our predictions for the velocity profile are compared with those of Erian & Tong (1971) by plotting $u_D/(\omega r_D)$ against $z_D\sqrt{(\omega/\nu)}$ as shown in figure 10 and display good agreement although there are clearly some slight differences. Similarly, although this is not illustrated here, our work shows reasonable agreement with the experimental data of Littell & Eaton (1994) and the LES of Wu & Squires (2000). In particular our predictions for the radial velocity component compare well with the findings of Littell & Eaton and Wu & Squires in the region of maximum radial velocity (Littell & Eaton predict a scaled radial velocity, $-W/U_\infty$, of approximately 0.105 for $Y/\delta_2 = 1$ compared to the value 0.11 predicted by our results); however the present predictions are seen to decay more rapidly with distance from the disk than has been noticed in these earlier works (for example Littell & Eaton predict a scaled radial velocity of approximately 0.043 for $Y/\delta_2 = 5.8$ compared to the value of approximately 0.03 predicted by our results). As mentioned earlier, the more rapid decay of the radial velocity seen in the current predictions is almost certainly a consequence of applying the boundary conditions at infinity at a finite value, t_∞, instead. The current numerical results are obtained by taking $t_\infty = 20$ and it is anticipated that increasing t_∞ would lead to slightly larger values of the radial velocity component as the distance from the disk increases.

Displacement thickness

Using the current numerical results it is possible to determine the displacement thickness δ_D^*, which is found to be

$$\delta_D^* = \epsilon g_{1\infty} k_1^2 r_D = 0.0347\epsilon r_D \tag{3.16}$$

https://doi.org/10.1017/S0022112007007550 Published online by Cambridge University Press

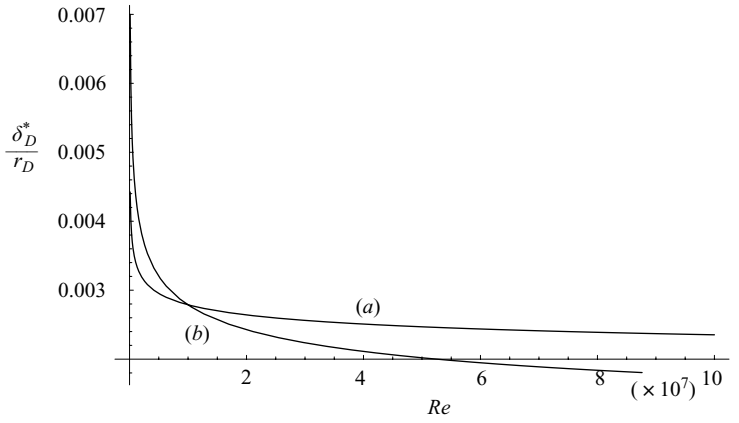


FIGURE 11. Comparison of the values predicted for the displacement thickness on a rotating disk between the present work (*a*) and that of Cooper (1971) (*b*).

as shown in figure 11. Our calculations for the displacement thickness can then be compared with Cooper (1971) for different values of the rotational Reynolds number R_r. In particular Cooper makes the prediction that $\delta_D^* = 0.0700(\nu/\omega)^{1/5} r_D^{3/5}$. This discrepancy may well arise from the inclusion of the intermittency factor in the work of Cooper although the use of a quasi-similarity solution here is more likely to be the crucial factor.

Skin friction

Finally, an analytical prediction for the skin friction on the disk is derived. The circumferential skin friction coefficient is defined as

$$c_{f\theta} = \frac{2\tau_{WD\theta}}{\rho(\omega r_D)^2} \quad \text{where} \quad \tau_{WD\theta} = \mu \left(\left| \frac{\partial v_D}{\partial z_D} \right| \right)_{z_D=0};$$

hence, following the same procedure as for the belt, the result

$$c_{f\theta} = 2k_1^2 \epsilon^2 \tag{3.17}$$

is obtained, which is the same as that for the skin friction coefficient on the moving belt and shows reasonable agreement with the findings of Cebeci & Abbott (1975) although our results are consistently lower.

Summary

The success of the present approach has been rather more varied when applied to a rotating disk as opposed to a moving belt. Our analytical prediction for the skin friction is again in good agreement with that of earlier work. Likewise our results compare reasonably well with the numerical work of Erian & Tong and the experimental findings of Littell & Eaton. Here it is worth repeating that a possible cause of these relatively minor inconsistencies may be the omission of intermittency from the present investigation (which was incorporated into Cooper 1971 and Cebeci & Abbott 1975). A more serious issue is the significant disparity between the predictions for the displacement thickness in the present work and Cooper (1971). This suggests that the use of a quasi-similarity solution here, whilst useful in reducing the problem to a simpler system, is generally inappropriate and that a fully two-dimensional treatment is required. Crucially, none of the analyses, in particular the behaviour of the flow in the laminar sublayer and the need for

https://doi.org/10.1017/S0022112007007550 Published online by Cambridge University Press

enhanced boundary layer thickness, is dependent on the use of such a quasi-similarity solution.

4. Further comments

The prime finding in the present theoretical work is that the induced flow thickness scales like k_1^2, the square of the von Kármán constant. The thickness is thus comparatively massive, being independent of the Reynolds number and implying a typical slope of about 0.16 for the induced streamlines. This significant and surprising finding is for the fully turbulent belt and disk flows in particular although it almost certainly applies to other motions occurring in the absence of an outer stream. Despite the action of wall drag and shear in the belt or disk flows examined here similar scales are found in free jets, although the present flow structure as well as the scales are quite distinct from those of turbulent motions with an external stream.

The work applies to general eddy viscosity models both for the planar moving belt and the axisymmetric rotating disk which are the fundamental configurations studied here. The rather more analytical approach used here appears to have generated encouraging predictions for the velocity profiles and skin friction, partly as they are in broad agreement with previous or empirical work on the rotating disk flow. The results for the displacement thickness are less so as they suggest that this measure of the flow thickness grows more rapidly than is seen in the von Kármán or Cooper scenarios, a difference which may well arise due to the quasi-similarity solution employed here. The relatively massive thickness of the flow overall, however, seems to be undeniable whether for the disk or the belt.

Given the flexibility and reasonable overall validity of the model and the assumptions made it would be interesting to apply the theory to rotor-blade and similar three-dimensional non-axisymmetric flow configurations.

Special thanks are due to Bernhard Scheichl for full and frank discussions; his research has independently arrived at a similar conclusion on flow thickness for a different but related configuration. These were supported by helpful comments from Alfred Kluwick. J.M.M. thanks EPSRC for financial support through a CASE award and both authors thank staff (in particular Roger Gent, Judith Miller, Mohammed Soliman and Colin Young) at QinetiQ for their interest.

REFERENCES

Afzal, N. 1996 Turbulent boundary layer on a moving continuous plate. *Fluid Dyn. Res.* **17**, 181–194.

Bhattacharrya, S. & Smith, F. T. 2003 Comparisons of direct simulations and analytical predictions for multi-plate flows. *Computers Fluids* **33**, 257–265.

Bowles, R. G. A. & Smith, F. T. 2000*a* Interactive flow past multiple blades and wakes. *Q. J. Mech. Appl. Maths* **53**(2), 207–251.

Bowles, R. G. A. & Smith, F. T. 2000*b* Lifting multi-blade flows with interaction. *J. Fluid Mech.* **415**, 203–226.

Bush, W. B. & Fendell, F. E. 1972 Asymptotic analysis of turbulent channel and boundary-layer flow. *J. Fluid Mech.* **56**, 657–681.

Cebeci, T. & Abbott, D. E. 1975 Boundary layers on a rotating disc. *AIAA J.* **13**, 829–832.

Clauser, F. H. 1956 The turbulent boundary layer. *Adv. Appl. Mech.* **IV**, 1–51.

Cooper, P. 1971 Turbulent boundary layer on a rotating disc calculated with an effective viscosity. *AIAA J.* **9**, 255–261.

https://doi.org/10.1017/S0022112007007550 Published online by Cambridge University Press

Davies, C. & Carpenter, P. W. 2003 Global behaviour corresponding to the absolute instability of the rotating-disc boundary layer. *J. Fluid Mech.* **486**, 287–329.

Davies, C., Thomas, C. & Carpenter, P. W. 2007 Global stability of the rotating-disc boundary ayer. *J. Engng Maths* (in press).

Erian, F. F. & Tong, Y. H. 1971 Turbulent flow due to a rotating disc. *Phys. Fluids* **14**, 2588–2591.

Gregory, N., Stuart, J. T. & Walker, W. S. 1955 On the stability of three-dimensional boundary layers with application to the flow due to a rotating disc. *Phil. Trans. R. Soc. Lond.* A **248**, 155–199.

Jones, M. A. & Smith, F. T. 2003 Fluid motion for car undertrays in ground effect. *J. Engng Maths* **45**, 309–334.

von Karman, Th. 1921 Laminare und Turbulente Reibung. *Z. Angew. Math. Mech.* **1**, Part 4, 233–252.

Launder, B. E. & Sharma, X. 1974 Application of the energy-dissipation model of turbulence to the calculation of flow near a spinning disc. *Lett. Heat Mass Transfer* **1**, 131–138.

Lingwood, R. J. 1995 Absolute instability of the boundary layer on a rotating disc. *J. Fluid Mech.* **29**, 17–33.

Lingwood, R. J. 1996 An experimental study of absolute instability of the rotating-disc boundary-layer flow. *J. Fluid Mech.* **314**, 373–405.

Littell, H. S. & Eaton, J. K. 1994 Turbulence characteristics of the boundary layer on a rotating disk. *J. Fluid Mech.* **266**, 175–207.

McDarby, J. M. 2004 Modelling of turbulent rotor-blade flow and ground effect. PhD thesis, University of London.

Mellor, G. L. 1972 The large Reynolds number, asymptotic theory of turbulent boundary layers. *Intl J. Engng Sci.* **10**, 851–873.

Neish, A. & Smith, F. T. 1988 The turbulent boundary layer and wake of an aligned flat plate. *J. Engng Maths* **22**, 15–42.

Prandtl, L. 1952 *Essentials of Fluid Dynamics*. Blackie & Son.

Purvis, R. & Smith, F. T. 2004 Planar flow past two or more blades in ground effect. *Q. J. Mech. Appl. Maths* **57**, 137–160.

Sakiadis, B. 1961*a* Boundary layer on continuous solid surface. I Boundary-layer equations for two-dimensional and axisymmetric flow. *AIChE J.* **7**, 26–27.

Sakiadis, B. 1961*b* Boundary layer on continuous solid surface. II The Boundary layer on a continuous flat surface. *AIChE J.* **7**, 221–225.

Scheichl, B. 2001 Asymptotic theory of marginal turbulent separation. PhD thesis, Vienna University of Technology.

Scheichl, B. & Kluwick, A. 2007*a* Turbulent marginal separation and the turbulent Goldstein problem. *AIAA J.* **45**, 20–36.

Scheichl, B. & Kluwick, A. 2007*b* A novel triple-deck problem for turbulent flows. *Progress in Turbulence II. Proc. iTi Conference on Turbulence 2005*. Proceedings in Physics, Vol. 109. Springer.

Schlichting, H. 1960 *Boundary Layer Theory*, 4th Edn. McGraw-Hill.

Smith, F. T. & Timoshin, S. N. 1996*a* Blade-wake interaction and rotary boundary layers. *Proc. R. Soc. Lond.* **452**, 1301–1329.

Smith, F. T. & Timoshin, S. N. 1996*b* Planar flows past thin multi-blade configurations. *J. Fluid Mech.* **324**, 355–377.

Speziale, C. G. & So, R. M. C. 1998 Turbulence modelling and simulation. In *The Handbook of Fluid Dynamics* (ed. R. W. Johnson). CRC Press.

Tsou, F. K., Sparrow, E. M. & Goldstein, R. J. 1967 Flow and heat transfer in the boundary layer on a continuous moving surface. *Intl J. Heat Mass Transfer* **10**, 219–235.

Wilcox, D. C. 1998 *Turbulence Modelling for CFD*, 2nd Edn. DCW Industries, Inc.

Wu, X. & Squires, K. D. 2000 Prediction and investigation of the turbulent flow over a rotating disk. *J. Fluid Mech.* **418**, 231–264.

Zandbergen, P. J. & Dijkstra, D. 1987 Von Karman swirling flows. *Annu. Rev. Fluid Mech.* **19**, 465–491.

https://doi.org/10.1017/S0022112007007550 Published online by Cambridge University Press